# Janus-Type Hybrid Paper Membranes

*Maximilian Nau, Nicole Herzog, Johannes Schmidt, Tobias Meckel, Annette Andrieu-Brunsen*, Markus Biesalski**

Maximilian Nau, Nicole Herzog, Dr. Tobias Meckel, Prof. Annette Andrieu-Brunsen, Prof. Markus Biesalski
Ernst-Berl Institut für Technische und Makromolekulare Chemie, Technische Universität Darmstadt, Alarich-Weiss-Strasse 4, D-64287, Darmstadt, Germany
E-mail: andrieu-brunsen@smartmem.tu-darmstadt.de
biesalski@tu-darmstadt.de

Dr. Johannes Schmidt
Fakultät II, Institut für Chemie, Technische Universität Berlin, Hardenbergstr. 40, D-10623 Berlin, Germany

Keywords: Janus membranes, hybrid materials, asymmetric material distribution, ultrathin coating, functional paper

Abstract: Functional paper-based materials and devices have been increasingly attractive to scientists in the recent past. In particular, the possibility to functionalize the surface of paper fibers with tailor-made coatings has broadened a possible scope of emerging application considerably. This work introduces novel functional paper membranes with adjustable gradient and Janus-type wettability based on gradient and Janus-type silica coating distribution along the paper cross-section. Correlation of CLSM (distribution), TGA (silica amount) and Kr-BET (surface area), reveals an extremely low coating thickness, in the range of just a few nanometers, being sufficient to fully inverse paper wettability from hydrophilic to very hydrophobic excluding water. This asymmetric wettability, originating from an asymmetric silica distribution along the paper cross section, is established by synchronizing silane hydrolysis and condensation reaction rates with silane transport rates in paper within a simple and scalable one-step drying process after having immersed a paper sheet into a tetraethoxysilane (TEOS) containing precursor-solution. As silica by itself, like paper, is a hydrophilic material the observed hydrophobicity is related to a reduction in cellulose fiber nanoscale porosity controlling water imbibition. While being relevant in manifold

applications, these ultrathin, Janus-type hybrid paper membranes are demonstrated to show directed gating and selective oil-water separation.

## 1. Introduction

In the recent past, research in various cross-disciplinary fields has been inspired by nature, and consequently, attempts to mimic material properties found in plants and animals are widespread. Natural cactus, spider silk, lotus leafs and desert beetles are some examples showing fascinating performance that is strongly based on their asymmetric physical structure or asymmetric chemical properties, both in bulk and in surface-confined coatings.[1-5] Referencing their two-faced nature, such asymmetric material properties often named after the Roman god Janus. In particular, the behavior of membranes, particles, rods, or micelles with two orthogonal sides shows high potential for different applications, such as oil/water separation, droplet manipulation, fog collection, unidirectional water flow design, bubble aeration, ion gating, and energy harvesting.[6-12] In particular, asymmetrically designed membranes show strong potential for improved transport design and thus improved application performance. Directed oil-water transport in the context of oil-water separation and directed gas-water transport in the context of fuel cell gas diffusion layers are two specific application examples.[13, 14] Therefore, enhancing control of material design and reducing the amount of material needed to achieve asymmetric material characteristics such as wettability are still an ongoing challenge. To make this situation even more stimulating, applying biocompatible and degradable materials while retaining needed stability and doing this in simple, ideally single-step, scalable fabrication processes are of increasing demand.

Janus materials in general are well known since the Nobel Prize lecture of de Gennes in 1991, but they were first mentioned in 1898 by the group of Veyssié.[15, 16] The general definition of Janus materials is diverse and includes all materials with asymmetric surfaces as well as composite bulk materials. In 2016, the group of Xu reshaped the definition of materials

having opposing properties at two respective interfaces and proposed three configurations of so-called Janus membranes.[5] One is the "A to B"-type material, which shows a physical and/or chemical gradient across a membrane cross-section. Alternatively, A-to-B or A- and B-type Janus membranes are defined as having a clear interface between the layers. Within the last few years, the Jiang group developed a coating and peeling strategy for the facile preparation of multifunctional Janus membranes based on synthetic polymers such as polyethylene terephthalate (PET)/polytetrafluoroethylene (PTFE).[1] After membrane modification by tannic acid (TA) and diethylenetriamine to form a hydrophilic coating on the surface, peeling off the top PTFE layer from the hydrophilic membrane results in a Janus membrane showing unidirectional water permeation properties at an oil/water interface.[1] Despite their interesting side-specific separation performance, these materials are fully synthetic with respect to their origin. In 2014, the group of Ikkala presented a membrane consisting of cotton modified on one side by chemical vapor deposition (CVD) of perfluorooctyltrichlorosilane, resulting in a Janus-type material via a single-step preparation.[8] These composite materials exhibit a directional gating to water droplets at the air-water interface as well as oil-water systems with integrated selectivity for oil or water inspired by the passive transport across cell membranes based on transmembrane hydrophilic/hydrophobic interactions.[17, 18] As demonstrated, for example, by the work of Ikkala, a hydrophobic interface can be designed by using silanes that chemically bind to the hydroxyl groups at the surface of cotton fibers. Control wetting through silane-based coatings has been a broad area of research since silanes represent a facile way to modulate the interfacial properties of surfaces.[19-24] Additionally, the utilization of PDMS in combination with silica particles on cellulose fibers has yielded some promising results in regards to mechanically stable coatings, a challenge that still faces a number of micro/nanostructured surfaces.[25, 26] While these strategies evidently have proven track records, the production of the material is rather laborious, including delicate sol/gel processes and the necessity for several

steps to produce the interface.[26, 27] In addition, the use of perfluorinated compounds in surface modification should raise concerns with respect to the environmental impact, especially if these coatings should be implemented on an industrial scale.[28] Furthermore, if silanes are implemented without the generation of a micro- or nanostructure, for example, on cellulosic substrates, the wettability of surfaces can only be modulated by alteration of the silane derivatives used and thus of the final surface energy of the chemically modified substrate.[29, 30] These techniques again all utilize a range of organo- and perfluorinated compounds.[31] Interestingly, a study from Cappelletto et al. on nonwoven cellulose fiber webs, such as paper, reports that coating tetraethoxysilane (TEOS) without further modification increases hydrophobicity. When relatively high silica amounts, namely, 20 and 40 wt.-% (by thermal analysis), were deposited on paper fibers, the static contact angle was increased; however, the samples were still classified as hydrophilic, and only the introduction of methyl-groups through the use of methyl-substituted precursors instead of TEOS led to hydrophobic materials.[32] Due to the large amounts of silica deposited, the fiber microstructure is consequently masked, and contact angle (CA) analysis effectively sampled a slightly structured silica surface rather than an open porous paper structure. An interesting application shown by Kehr and Motealleh in 2017 was the use of Janus-type paper sheets as a three-dimensional (3D) cell culture system.[33] Spatially resolved functionalization of the paper substrate is not reported with this particular strategy. However, for any successful design of Janus-type (paper-based) membranes, gradients of the surface chemistry within the substrate are perhaps the key parameter to guide wettability within defined areas of the hybrid material. Here, we present a novel cellulose-based hybrid material that addresses the above outlined challenges of known Janus-type membranes through a facile production method using a single-step process. Highly controlled deposition of very small amounts of silica on lab-engineered paper substrates enables us to avoid the use of perfluorinated or organo-modified

silanes, providing a cheap, easy, sustainable and biobased route to generate highly functional asymmetric, i.e., Janus-type, hybrid materials.

## 2. Results and Discussion

To design Janus-type paper hybrid materials with asymmetric wettability and capillary-driven fluid flow, we modified lab-engineered eucalyptus sulfate paper with extremely low amounts of silica. Asymmetric silica coating distribution and thus wetting and fluid flow gradients are achieved through a dip-coating process in a tetraethoxysilane (TEOS)-containing ethanol-water-based solution, adapted from our prior work, together with a subsequent heat treatment at 130 °C at atmospheric pressure or at reduced pressure (**Figure 1a-**c).[34] The temperature of 130 °C was chosen because it is known to be nondestructive to eucalyptus paper while allowing acid (i.e., HCl)-catalyzed hydrolysis and condensation of TEOS, resulting in silica formation.[34, 35] By using a simple dip-coating process and tuning the initial TEOS concentration in the coating solution, the wetting characteristics progress from hydrophilic to Janus type and hydrophobic in a controlled fashion by adjusting a precise and simple gradient design. Investigation by eye, microscope, and SEM did not show macroscopic changes in the eucalyptus paper structure or alterations on the micrometer scale (**Figure 1** b) and c)) compared to unmodified paper sheets (**Figure 1** a)). This apparent lack of discernible topographical and morphological differences indicates that the relevant features of the coating and its thickness must be smaller than the resolution limit of the SEM under the given conditions (2500x/76 $nm^2$). In comparison, the work of Cappelletto et al. showed obvious masking of the paper structure already when 20 wt.-% silica was applied to paper surfaces and still yielded materials considered hydrophilic.[32] Unfortunately, SEM nanoscale analysis of the silica-coated eucalyptus paper sheets is not trivial due to the high energy needed for imaging, which can destroy the organic matrix of the hybrid material. Consequently, further studies are

conducted via correlated TGA, CLSM and BET analysis to gather information at the submicron scale.

Macroscopic static contact angle (CA) measurements of the top and bottom surfaces of all silica-coated eucalyptus sulfate paper samples (**Figure 2**) prepared in this study were carried out to study the influence of the silica coating on the wetting behavior of the hybrid paper. All samples prepared with high TEOS concentrations (for solution composition, please refer to the experimental section) exhibit hydrophobic wetting characteristics with static contact angles of 120°-130°. Note that the chemical surface of cured TEOS is composed solely of hydrophilic hydroxyl functions. No difference between the macroscopic static water contact angles of the top and bottom surface is observed, regardless of the orientation during curing and curing pressure, i.e. ambient pressure vs. vacuum oven. In contrast, all eucalyptus paper sheets coated with low TEOS concentrations in the dip-coating process do exhibit hydrophilic wetting behavior. We found no difference between top versus bottom side wetting behavior nor any differences in the wetting of the hybrid materials using the two different curing strategies (at atmospheric pressure vs. under reduced pressure). Interestingly, the eucalyptus paper sheets coated with intermediate TEOS concentrations show a very different and curing process-dependent wetting behavior: if these samples are cured in an oven under ambient pressure, the top side exhibits hydrophobic wetting behavior with static contact angles of approximately 120°, whereas the bottom side exhibits hydrophilic macroscopic static contact angles of 0° along with water exclusion at the top side and instant and complete water imbibition at the bottom side (**Figure 2** blue). As the top surface is water repellent, while the bottom side absorbs water immediately, a Janus-type or amphiphilic membrane has been created. This result can be explained by the positioning of the sample in the oven and by considering migration of the TEOS during the drying procedure. The sample is placed in an oven during drying in a horizontal position (**Figure 1**b), favoring a directed migration of

TEOS due to the preferred ethanol evaporation at the top of the paper sheet. If ethanol evaporation and silane hydrolysis as well as condensation now occur on similar time scales, a gradient in silica distribution along the eucalyptus paper cross-section is obtained. Curing eucalyptus paper sheets coated with identical intermediate TEOS concentrations in an oven under reduced pressure results in hydrophilic wetting behavior on both sides of the paper sheets. This result can be explained by the fact that evaporation of the solvent is now much faster than migration of TEOS, and thus, homogeneous paper characteristics with respect to the silica coating are obtained.

To understand the findings outlined above in more detail, we next addressed the following questions: how much silica is deposited on the respective paper sheets, what does the silica distribution look like and is there an effective coating thickness necessary in order to achieve hydrophobic wetting characteristics?

The amount of deposited silica within the eucalyptus paper sheet was determined via TGA (**Figure 3**). Due to the apparently very low amount of silica, TGA is the method of choice because of the very small errors compared to those of alternative methods such as standard gravimetric analysis, especially for small sample amounts. During a TGA measurement, the silica content of coated paper sheets was determined by thermal removal of the paper, which only leaves silica (stable up to 1700 °C) and ash. The determined amount of silica is calculated considering the ash content, 5.8 wt.-%, of the base paper deduced from a reference measurement. This finding shows that the silica content in the low TEOS concentration coated papers is 0.5 wt.-%; in the intermediate TEOS concentration coated papers, 1.5 wt.-%; and in the high TEOS concentration coated papers, approximately 3.7 wt.-% (**Table S1**, ESI).

Further analysis using Krypton sorption reveals a specific surface area (BET) for uncoated samples of 0.54 $m^2/g$. While eucalyptus fiber macropores are unaffected by the

aforementioned silica coating, as is evident through SEM imaging (**Figure 1**), the Kr-BET specific surface area progressively changed from 0.59 $m^2/g$ (low), over 0.43 $m^2/g$ (intermediate), to 0.27 $m^2/g$ (high).

This decrease in surface area, indicates that the mechanism of the silica induced hydrophobization is not based on the generation of micro- or nano structure. Mechanistically, we rather suggest a mechanism based on pinning on the 3-phase contact line on the micro-rough paper which is facilitated through the fact that coated fibers cannot undergo subsequent swelling of the cellulosic material. The pinning mechanism, with respect to water on hydrophilic surfaces has been described in detail by Hensel et al. and is facilitated through the inhibition of fiber swelling and masking of the internal and external fiber surface.[36] This hypothesis is supported by a rather miniscule decrease in free surface energy from cellulose (63.8 mN/m) to silica (59.2 mN/m) that were determined on model surfaces (**Table S2**, ESI).

2.1. Silica-distribution analysis

To further explain the Janus paper characteristics, we determined the cross-sectional silica distribution to address possible threshold concentrations of silica deposited at the fiber surfaces that is need to render the hybrid material hydrophobic (i.e., where no further wicking of a water drop into the material can be observed). The relative silica distribution is obtained by using CLSM imaging. This technique is based on our prior investigations regarding localized modifications of paper and functionalization of fiber surfaces.[37, 38] Examples of CLSM image stacks of cross-sections of the hybrid paper material are displayed in **Figure 4**. The untreated cellulose sheets were stained with Calcofluor white prior to dip-coating with rhodamine B-labeled silica precursor solution. The silica (rhodamine B channel) is colored magenta, while the eucalyptus fibers (CFW channel) are colored cyan.

For the three different TEOS concentrations applied during dip-coating (compare **Figure 4** a-c and **Figure 4** d-f) and the two curing methods (ambient pressure and reduced pressure, **Figure 4** a,d; b,e; c,f), similar silica distributions are observed (**Figures S1** and **S2**, ESI). TEOS-coated eucalyptus paper sheets cured under vacuum show bathtub-like silica distribution along the cross-section with an increased silica amount at the top and bottom surfaces of the paper cross-section (**Figure S1**, ESI). The relative difference in deposited silica between the outer paper sheet surfaces and the center of the cross-section increases with decreasing TEOS concentration in the dip-coating solution. This result implies that the TEOS concentration within the coating solution affects the movement of the liquid phase during TEOS hydrolysis and condensation, e.g., via changes in the fluidic properties (e.g., viscosity) and different interactions with the fibrous eucalyptus paper substrate.

On the other hand, eucalyptus paper sheets cured under ambient pressure show up to two times higher relative silica concentration on the top of the samples than on the bottom. The silica gradient along the cross-section of the hybrid paper is less pronounced if the initial coating solution contains higher TEOS concentrations. The reason for this behavior again can be found in the evaporation kinetics, and thus, the relation of material transport with hydrolysis-condensation speed determines the chemical gradient formation of the silica-modified hybrid paper. (**Figure S1** and **S2**, ESI).

To gain further insight into the absolute mass distributions, the relative measurements are numerically integrated (over the cross section) and normalized, and the relative partial integral for each 10 µm cross-section segment of the paper sheet cross-section is calculated and multiplied by the coating weight, as determined by TGA. This procedure allows us to determine the distribution of absolute volumetric coating weights, as displayed in **Figure 5**a (cured under vacuum) and **Figure 5**b (cured under ambient pressure). By correlating the obtained silica distribution with the static CA values described above, a correlation between the silica amount and wetting is observed: The threshold silica amount above which the paper

sheet becomes hydrophobic is located between the highest coating weight (still resulting in hydrophilic wetting) and the lowest silica coating weight (just inducing hydrophobic wetting). The highest amount of silica in a hydrophilic sample (lower threshold boundary) is observed with the top surface of the samples coated with the intermediate TEOS concentration and cured under vacuum (**Figure 5**a, blue), while the lowest already hydrophobic material is observed with the corresponding sample cured under atmospheric pressure (**Figure 5**b, blue). While the sample cured under atmospheric pressure is still hydrophobic with a specific coating weight of 10.3 mg $cm^{-3}$ (**Figure 5**b), the sample cured under vacuum is hydrophilic at a specific coating weight of 9.3 mg $cm^{-3}$ (**Figure 5**a), which defines the threshold between those two boundaries. Consequently, a minimum silica content between 1.85 wt% and 2.05 wt% with respect to eucalyptus sulfate fibers is necessary to obtain hydrophobic hybrid membrane behavior. In brief, we determined a minimal threshold amount of TEOS coating, which is necessary to induce the hydrophobic effect, samples prepared from low-TEOS concentration, as shown by the data in Figure 5 did not overcome this threshold amount on either surface and thus remained hydrophilic, indicating our data to be accurate. Through correlation of these data with the Kr-BET specific surface area, the threshold in terms of coating weight is located between about 43 and 47 mg/m², respectively. The apparent absence of changes in the micrometer scale is subsequently self-explanatory because the density of silica (2.65 g/cm²) corresponds to - with respect to paper coatings - ultrathin coating thicknesses between 16 and about 18 nm, respectively.

## 2.2. Application of TEOS-modified paper as tunable membrane

To show the versatility of asymmetric paper-based Janus membranes, we demonstrate their ability to separate oil and water as one possible application model. For this purpose, a two-phase water-oil system consisting of water and cyclohexane was used. Cyclohexane was chosen as an oil component to eliminate effects based on high viscosity. The investigated

paper sheet is located at the interface between water and cyclohexane (**Figure 6**b). Through use of the three different TEOS concentrations for eucalyptus paper coating and facile orientation, all possible permeation combinations for this system can be designed, as depicted in **Figure 6**a. The paper sheets coated with "low" and "high" amounts of TEOS behave as expected. If a FITC-labeled water drop is placed onto the hydrophilic paper membrane (i.e., "low" TEOS coating, **Figure 6**e), the latter allows water permeation, as easily inferred even by the naked eye. However, the same membrane does not allow any visible permeation of the nonpolar oil. The opposite behavior is observed for the hydrophobic paper (i.e., "high" TEOS coating, **Figure 6**d): The Sudan IV-labeled oil droplet is capable of permeating the fibrous network, whereas the water droplet does not penetrate the surface of the paper. Most interestingly, however, the Janus-type paper (i.e., the "intermediate" TEOS coating dried under ambient pressure) is acting as a "double diode": Both water and oil are capable of permeating through the membrane but only with a specific direction and in opposite directions relative to each other (**Figure 6**c,f). This property prohibits reverse permeation, as demonstrated by the fact that one orientation of the Janus paper (hydrophobic side facing towards the water, **Figure 6**c) will let water pass through from the oil side, and vice versa. In the opposite orientation (hydrophobic side facing towards the oil, **Figure 6**f), permeation is blocked in both directions. Note, investigation of the influence of geometric factors of the hydrophobic coating (i.e. thickness) on the permeation dynamics is a complex endeavor to be addressed in follow-up scientific studies. However, comparable properties have, to the best of our knowledge, only been realized using fluorosilanes, dodecanethiol, poly(dimethylsiloxane) (PDMS) or polymers such as polyethylene terephthalate (PET) and polytetrafluoroethylene (PTFE) obtained through multistep, sophisticated processes. The approach presented here essentially produces paper coated with an extremely low amount of silica (i.e., $SiO_2$) content using nothing but an oven heated to 130 °C.[1, 5, 8, 39-41] Moreover, due to the ease of

application, even a simple scale-up to roll-to-roll coating shall in principle be possible, given the state of art technologies in papermaking and printing.

## 3. Conclusion

This work presents a facile, sustainable, and scalable method to create paper-based hybrid materials with designed wettability and wettability gradients ranging from very hydrophilic to fully hydrophobic. Especially paper-based hybrid membranes with Janus-type asymmetric wetting characteristics using extremely low amounts of TEOS as the only active chemical in a simple dip-and-cure process are provided. These asymmetric wetting characteristics are based on an interplay of silane reactivity and environment-controlled transport along the paper cross-section during curing. This simple process allows for tailored adjustment of the silica gradient across the paper cross-section. This inherently simple and easily scalable process produces thin silica coatings on the outer, as well as on the inner surface of the cellulose fibers within the paper sheet. The silica coating amount can be precisely adjusted through variation in the TEOS concentration in the initial coating solution together with control of the curing conditions, especially the air pressure, employed during the curing step. It has to be emphasized that an extremely low silica coating amount (1.40 – 3.70 wt.-%, with respect to the final membrane mass) results in fully hydrophobic as well as Janus-type wetting characteristics, as determined by the correlation of CLSM, TGA and BET analysis, respectively. Thereby a low silica content of 1.85-2.05 wt.-% is sufficient to produce a hydrophobic interface on eucalyptus paper, by generating localized coating thicknesses of just a few nanometers. Mechanistically the observed hydrophobization is based on nanoscale porosity reduction. The generated A-B Janus-type paper sheets are capable of separating oil and water in a double-diode fashion, allowing permeation of water from one side and permeation of oil from the opposite side and in opposite directions. The latter offers great potential for the design of simple yet efficient oil-water separation membranes for future

water management concepts. In contrast to state-of-the-art membrane designs known today, our membranes consist of fully bio-based compounds and can be easily disintegrated and recycled using well-established technologies with paper recycling. Finally, a simple scale-up to roll-to-roll coating will in principle be possible, given the technologies in papermaking and printing.

## 4. Experimental Section

*Reagents*: All chemicals and solvents were purchased from Fisher Scientific, Merck, Sigma-Aldrich or Alfa Aesar and used as received unless otherwise stated.

*Paper Fabrication:* For the preparation of lab-engineered paper substrates, eucalyptus sulfate pulp (curl: 16.2 %; fibrillation degree: 1.3 %; fines content: 15.2 %) was used. The pulp was refined in a Voith LR 40 laboratory refiner. Refining was performed with an effective specific energy of 16 kWh $t^{-1}$ (750000 revolutions). Laboratory-engineered paper substrates were prepared from said pulp with a grammage of 80 ± 0.9 g $m^{-2}$ by using a Rapid-Köthen sheet former according to DIN 54358 and ISO 5269/2 (REF: ISO 5269-2:2004(E), Pulps – Preparation of Laboratory Sheets for Physical Testing – Part 2: Rapid Köthen Method, 2004.) No additives or filler materials were used. Prior to coating, the paper was conditioned for at least 24 h under standard conditions (23 °C, 50 % r.h.).

*Silica Coatings:* Silica coatings were generated from three TEOS-containing dip-coating solutions that were prepared with the following molar ratios: The color code remains consistent throughout the work.

1 TEOS : 80 EtOH : 20 H2O : 0.04 HCl → low concentration

1 TEOS : 40 EtOH : 10 H2O : 0.02 HCl → intermediate concentration

1 TEOS : 20 EtOH : 5 H2O : 0.01 HCl → high concentration

The precursor solutions were stirred at 22 °C for 24 h and subsequently used for dip-coating on eucalyptus sulfate paper strips (1 cm* 8 cm) at 50 % relative humidity and 23 °C at a withdrawal speed of 2 mm $s^{-1}$. After dip-coating, samples were directly brought into a 130 °C preheated vacuum curing oven or a muffle furnace that was heated from 23 °C to 130 °C. The samples were kept at 130 °C for 2 h (regardless of the heating method) before cooling to ambient temperature. The samples are marked on the top side (with respect to the orientation during the curing process) of the sheets.

*Contact Angle (CA):* Contact angle measurements were carried out using a Model TBU90E from DataPhysics Instruments GmbH with the corresponding software. All samples were measured at five positions, and the average value was calculated with standard deviation. For macroscopic static contact angle measurements, a water drop volume of 2 µL was used (dispense rate: 1 µL $s^{-1}$). To determine the surface energy of silica and regenerated cellulose, the macroscopic static contact angles on planar model surfaces (silica coating on a glass substrate and regenerated cellulose) were determined for different solvents. The following solvents with different surface energies were used: water, N,N-dimethylformamide, dimethyl sulfoxide, n-hexane and toluene. Subsequently, the respective surface energies of the model surfaces were calculated according to the Owens, Wendt, Rabel & Kälble (OWRK) method.

*Thermogravimetric analysis (TGA):* TGA analysis was performed on a TGA 1 instrument (Mettler−Toledo). The samples were heated from 25 °C to 600 °C at a rate of 10 K $min^{-1}$ under a constant air flow of 30 mL $min^{-1}$.

*Scanning Electron Microscopy (SEM):* Scanning electron microscopy (SEM) micrographs were acquired using a Philips XL30 FEG scanning electron microscope operated at an acceleration voltage of 10 kV. Samples were sputtered with a platinum(80)/palladium(20) layer of 10 nm prior to analysis.

*Preparation of the paper samples for CLSM:* The paper samples for CLSM analysis were coated with different amounts of TEOS in the same fashion as described before except for the

addition of fluorescence labels. For this purpose, the untreated paper was dip-coated in an ethanol (abs.) solution of 10 µM Calcofluor white (CFW). After drying at 40 °C in a vacuum oven (Heraeus, VTR 5036) for 1 h, the resulting CFW-labeled samples were coated with silica as described before except for the addition of 20 µM rhodamine B (based on the amount of ethanol (abs.)) to the dip-coating solutions.

*Preparation of the cross-sections:* Each sample was embedded in a mixture of 49.9875 wt.% Desmodur® 3200, 49.9875 wt.% Albodur® 956 VP and 0.025 wt.% TIB-KAT 318, which is a commercial polyurethane system. The freshly embedded samples then underwent several vacuum cycles at room temperature to remove residual air bubbles; afterwards, the resin was cured for 18 h at 40 °C. The final semiflexible sample was then cut into 120 µm slices using a microtome. During all these steps, the identity of the "top" side was tracked via appropriate sample labeling.

*CLSM imaging:* The microtome-cut sample slices were placed between two 25 mm round microscope cover glasses Type No. 1 from "Assistent" in a custom sample holder. Optical matching was achieved using Type F immersion liquid from Leica. The imaging was performed on a Leica TCS SP8. The image stacks obtained for each sample were summed up to condense the information about the material distribution. A gray value analysis was performed on these summed image data for each row of pixels; i.e. the gray values of each image were added for every single pixel column. This procedure yields the relative distribution of the given material throughout the paper from top to bottom or, in terms of the images displayed in **Figure 4**, from left to right.

*Analysis of oil/water accessibility of paper membranes:* Water was placed in a cylindrical beaker, and the sample membrane was placed on the interface and covered with cyclohexane (oil simulant), as inspired by the work of Wang et al.[1] The beaker was positioned on top of a 365 nm lamp for excitation of fluorescein. A drop of cyclohexane colored with the dye Sudan IV was added through the water phase to the membrane, and a drop of water colored with

FITC-dextran was placed onto the membrane at the oil phase side. The experiment was recorded using a Canon EOS 700D camera equipped with a 55-250 mm objective and a 24 mm spacer ring.

*Krypton adsorption:* Krypton adsorption measurements were performed at 77 K using an Autosorb iQ2 from Quantachrome. The samples were degassed for 12 h prior to measurement, and the surface area was calculated from the Brunauer–Emmett–Teller (BET) model by selecting adsorption points satisfying the consistency criteria for application of the BET theory.

**Supporting Information**
Supporting Information is available from the Wiley Online Library or from the author.

Acknowledgements

We would like to thank Martin Brodrecht (Buntkowsky Group, Technische Universität Darmstadt) for the fruitful discussion and insight regarding BET-Analysis. We acknowledge fruitful collaboration within the framework DFG PAK 962 “Geometrische und Chemische Struktur funktionaler Papiere”.

Received: ((will be filled in by the editorial staff))
Revised: ((will be filled in by the editorial staff))
Published online: ((will be filled in by the editorial staff))

References

1. Wang, Z.; Yang, X.; Cheng, Z.; Liu, Y.; Shao, L.; Jiang, L., Simply realizing “water diode” Janus membranes for multifunctional smart applications. *Materials Horizons* **2017,** *4* (4), 701-708.
2. Walther, A.; Müller, A. H. E., Janus Particles: Synthesis, Self-Assembly, Physical Properties, and Applications. *Chem. Rev.* **2013,** *113* (7), 5194-5261.
3. Tian, X.; Li, J.; Wang, X., Anisotropic liquid penetration arising from a cross-sectional wettability gradient. *Soft Matter* **2012,** *8* (9).
4. Shah, A. A.; Schultz, B.; Zhang, W.; Glotzer, S. C.; Solomon, M. J., Actuation of shape-memory colloidal fibres of Janus ellipsoids. *Nat. Mater.* **2015,** *14* (1), 117-24.
5. Yang, H. C.; Hou, J.; Chen, V.; Xu, Z. K., Janus Membranes: Exploring Duality for Advanced Separation. *Angew. Chem. Int. Ed. Engl.* **2016,** *55* (43), 13398-13407.
6. Zhang, H.; Hou, X.; Zeng, L.; Yang, F.; Li, L.; Yan, D.; Tian, Y.; Jiang, L., Bioinspired artificial single ion pump. *J. Am. Chem. Soc.* **2013,** *135* (43), 16102-10.

7. Cao, M.; Ju, J.; Li, K.; Dou, S.; Liu, K.; Jiang, L., Facile and Large-Scale Fabrication of a Cactus-Inspired Continuous Fog Collector. *Adv. Funct. Mater.* **2014,** *24* (21), 3235-3240.
8. Tian, X.; Jin, H.; Sainio, J.; Ras, R. H. A.; Ikkala, O., Droplet and Fluid Gating by Biomimetic Janus Membranes. *Adv. Funct. Mater.* **2014,** *24* (38), 6023-6028.
9. Zhang, M.; Wang, L.; Hou, Y.; Shi, W.; Feng, S.; Zheng, Y., Controlled Smart Anisotropic Unidirectional Spreading of Droplet on a Fibrous Surface. *Adv. Mater.* **2015,** *27* (34), 5057-62.
10. Zhang, Z.; Kong, X. Y.; Xiao, K.; Liu, Q.; Xie, G.; Li, P.; Ma, J.; Tian, Y.; Wen, L.; Jiang, L., Engineered Asymmetric Heterogeneous Membrane: A Concentration-Gradient-Driven Energy Harvesting Device. *J. Am. Chem. Soc.* **2015,** *137* (46), 14765-72.
11. Yang, H.-C.; Hou, J.; Wan, L.-S.; Chen, V.; Xu, Z.-K., Janus Membranes with Asymmetric Wettability for Fine Bubble Aeration. *Adv. Mater. Interfaces* **2016,** *3* (9).
12. Yang, H. C.; Xie, Y.; Hou, J.; Cheetham, A. K.; Chen, V.; Darling, S. B., Janus Membranes: Creating Asymmetry for Energy Efficiency. *Adv. Mater.* **2018,** *30* (43), e1801495.
13. Forner-Cuenca, A.; Biesdorf, J.; Gubler, L.; Kristiansen, P. M.; Schmidt, T. J.; Boillat, P., Engineered Water Highways in Fuel Cells: Radiation Grafting of Gas Diffusion Layers. *Adv. Mater.* **2015,** *27* (41), 6317-6322.
14. Zhang, Z.; Wen, L.; Jiang, L., Bioinspired smart asymmetric nanochannel membranes. *Chem. Soc. Rev.* **2018**.
15. de Gennes, P.-G., Soft Matter (Nobel Lecture). *Angew. Chem. Int. Ed. Engl.* **1992,** *31*, 842-845.
16. Casagrande, C.; Fabre, P.; Raphael, E.; Veyssié, M., Janus Beads: Realization and Behaviour at Water/Oil Interfaces. *Europhys. Lett.* **1989,** *9* (3), 251-255.
17. Seddon, A. M.; Casey, D.; Law, R. V.; Gee, A.; Templer, R. H.; Ces, O., Drug interactions with lipid membranes. *Chem. Soc. Rev.* **2009,** *38* (9), 2509-2519.
18. Sugano, K.; Kansy, M.; Artursson, P.; Avdeef, A.; Bendels, S.; Di, L.; Ecker, G. F.; Faller, B.; Fischer, H.; Gerebtzoff, G.; Lennernaes, H.; Senner, F., Coexistence of passive and carrier-mediated processes in drug transport. *Nature Reviews Drug Discovery* **2010,** *9*, 597.
19. Hikita, M.; Tanaka, K.; Nakamura, T.; Kajiyama, T.; Takahara, A., Super-Liquid-Repellent Surfaces Prepared by Colloidal Silica Nanoparticles Covered with Fluoroalkyl Groups. *Langmuir* **2005,** *21* (16), 7299-7302.
20. Yang, H.; Liang, F.; Chen, Y.; Wang, Q.; Qu, X.; Yang, Z., Lotus leaf inspired robust superhydrophobic coating from strawberry-like Janus particles. *Npg Asia Mater.* **2015,** *7*, e176.
21. Xia, B.; Yan, L.; Li, Y.; Zhang, S.; He, M.; Li, H.; Yan, H.; Jiang, B., Preparation of silica coatings with continuously adjustable refractive indices and wettability properties via sol–gel method. *RSC Adv.* **2018,** *8* (11), 6091-6098.
22. Liu, D.; Wu, Q.; Andersson, R. L.; Hedenqvist, M. S.; Farris, S.; Olsson, R. T., Cellulose nanofibril core–shell silica coatings and their conversion into thermally stable nanotube aerogels. *J. Mater. Chem. A* **2015,** *3* (30), 15745-15754.
23. Xu, Q. F.; Wang, J. N.; Sanderson, K. D., A general approach for superhydrophobic coating with strong adhesion strength. *J. Mater. Chem.* **2010,** *20* (28), 5961-5966.
24. Chen, P.-H.; Hsu, C.-C.; Lee, P.-S.; Lin, C.-S., Fabrication of semi-transparent super-hydrophobic surface based on silica hierarchical structures. *J Mech Sci Technol 25*, 43-47.
25. Ke, Q. P.; Fu, W. Q.; Jin, H. L.; Zhang, L.; Tang, T. D.; Zhang, J. F., Fabrication of mechanically robust superhydrophobic surfaces based on silica micro-nanoparticles and polydimethylsiloxane. *Surf. Coat. Technol.* **2011,** *205* (21-22), 4910-4914.

26. Kosak Soz, C.; Trosien, S.; Biesalski, M., Superhydrophobic Hybrid Paper Sheets with Janus-Type Wettability. *ACS Appl. Mater. Interfaces* **2018,** *10* (43), 37478-37488.
27. Cai, S.; Zhang, Y.; Zhang, H.; Yan, H.; Lv, H.; Jiang, B., Sol–Gel Preparation of Hydrophobic Silica Antireflective Coatings with Low Refractive Index by Base/Acid Two-Step Catalysis. *ACS Appl. Mater. Interfaces* **2014,** *6* (14), 11470-11475.
28. Stahl, T.; Mattern, D.; Brunn, H., Toxicology of perfluorinated compounds. *Environ. Sci. Eur.* **2011,** *23* (1), 38.
29. Ding, B.; Li, C.; Hotta, Y.; Kim, J.; Kuwaki, O.; Shiratori, S., Conversion of an electrospun nanofibrous cellulose acetate mat from a super-hydrophilic to super-hydrophobic surface. *Nanotechnology* **2006,** *17* (17), 4332-4339.
30. Vasiljević, J.; Gorjanc, M.; Tomšič, B.; Orel, B.; Jerman, I.; Mozetič, M.; Vesel, A.; Simončič, B., The surface modification of cellulose fibres to create super-hydrophobic, oleophobic and self-cleaning properties. *Cellulose* **2013,** *20* (1), 277-289.
31. Ferrero, F.; Periolatto, M., Application of fluorinated compounds to cotton fabrics via sol–gel. *Appl. Surf. Sci.* **2013,** *275*, 201-207.
32. Cappelletto, E.; Callone, E.; Campostrini, R.; Girardi, F.; Maggini, S.; della Volpe, C.; Siboni, S.; Di Maggio, R., Hydrophobic siloxane paper coatings: the effect of increasing methyl substitution. *J. Sol-Gel Sci. Technol.* **2012,** *62* (3), 441-452.
33. Kehr, N. S.; Motealleh, A., Nanocomposite (Janus) paper as 3D cell culture system. *Colloids Surf., B* **2017,** *156*, 236-242.
34. Dubois, C.; Herzog, N.; Ruttiger, C.; Geissler, A.; Grange, E.; Kunz, U.; Kleebe, H. J.; Biesalski, M.; Meckel, T.; Gutmann, T.; Gallei, M.; Andrieu-Brunsen, A., Fluid Flow Programming in Paper-Derived Silica-Polymer Hybrids. *Langmuir* **2017,** *33* (1), 332-339.
35. De, G.; Karmakar, B.; Ganguli, D., Hydrolysis–condensation reactions of TEOS in the presence of acetic acid leading to the generation of glass-like silica microspheres in solution at room temperature. *J. Mater. Chem.* **2000,** *10* (10), 2289-2293.
36. Hensel, R.; Helbig, R.; Aland, S.; Braun, H.-G.; Voigt, A.; Neinhuis, C.; Werner, C., Wetting Resistance at Its Topographical Limit: The Benefit of Mushroom and Serif T Structures. *Langmuir* **2013,** *29* (4), 1100-1112.
37. Bump, S.; Böhm, A.; Babel, L.; Wendenburg, S.; Carstens, F.; Schabel, S.; Biesalski, M.; Meckel, T., Spatial, spectral, radiometric, and temporal analysis of polymer-modified paper substrates using fluorescence microscopy. *Cellulose* **2015,** *22*, 73-88.
38. Janko, M.; Jocher, M.; Boehm, A.; Babel, L.; Bump, S.; Biesalski, M.; Meckel, T.; Stark, R. W., Cross-Linking Cellulosic Fibers with Photoreactive Polymers: Visualization with Confocal Raman and Fluorescence Microscopy. *Biomacromolecules* **2015,** *16* (7), 2179-87.
39. Ren, F.; Li, G.; Zhang, Z.; Zhang, X.; Fan, H.; Zhou, C.; Wang, Y.; Zhang, Y.; Wang, C.; Mu, K.; Su, Y.; Wu, D., A single-layer Janus membrane with dual gradient conical micropore arrays for self-driving fog collection. *J. Mater. Chem. A* **2017,** *5* (35), 18403-18408.
40. Ju, J.; Xiao, K.; Yao, X.; Bai, H.; Jiang, L., Bioinspired conical copper wire with gradient wettability for continuous and efficient fog collection. *Adv. Mater.* **2013,** *25* (41), 5937-42.
41. Cao, M.; Xiao, J.; Yu, C.; Li, K.; Jiang, L., Hydrophobic/Hydrophilic Cooperative Janus System for Enhancement of Fog Collection. *Small* **2015,** *11* (34), 4379-84.

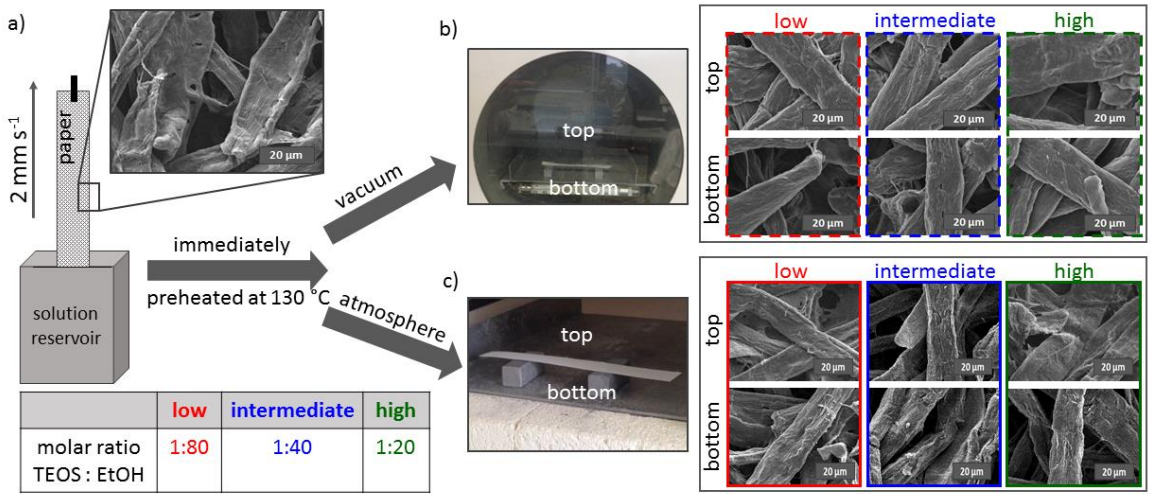


**Figure 1.** a) Schematic illustration of the preparation of silica-coated paper sheets. The paper sheet is dip-coated in three different precursor solutions having defined amounts of dissolved TEOS given in the inserted table. Subsequently, the samples are cured in preheated ovens at 130 °C under b) vacuum and c) atmospheric pressure, respectively. The inserted scanning electron microscopy images show examples of nonmodified eucalyptus sulfate paper (80 g/m², a)) and silica-modified eucalyptus-sulfate paper (80 g $m^{-2}$, b) and c)).

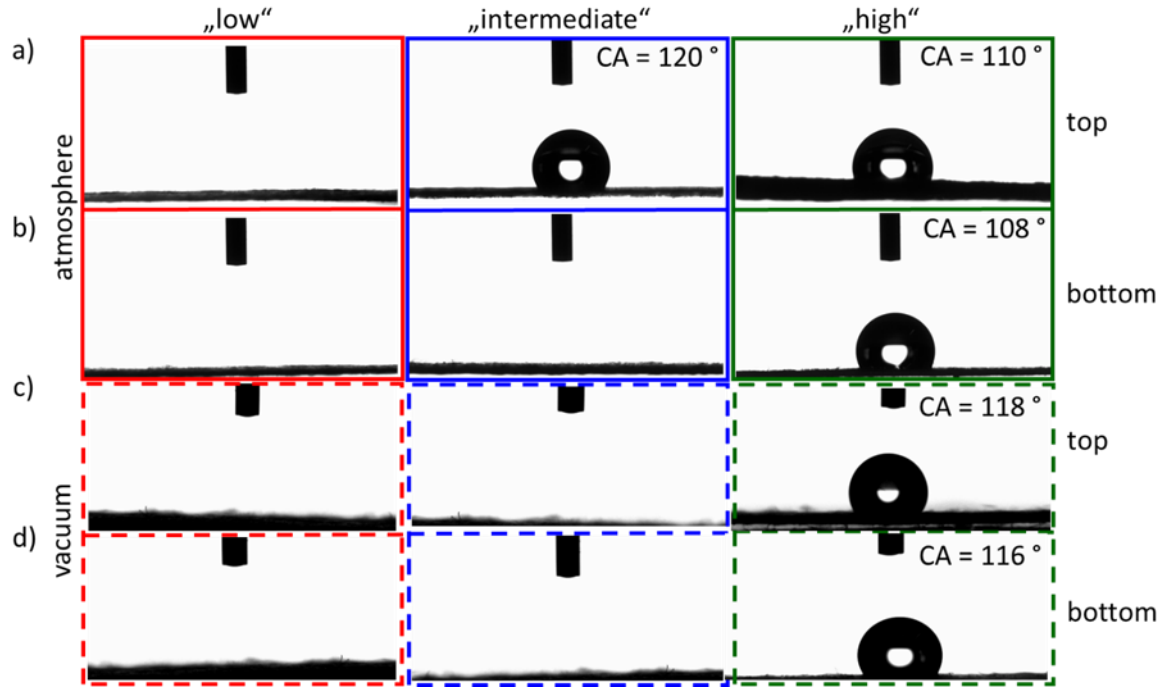


**Figure 2.** Static contact angle measurements of 2 µL water (MilliQ) droplets on silica-coated eucalyptus-sulfate paper sheets (~80 g $m^{-2}$). The papers were coated with the three different TEOS concentrations, “low”, “intermediate”, and “high”. a) shows the top surface and b) the bottom side of the paper after curing in a preheated oven, c) shows the top surface and d) the bottom side of the paper after curing in a vacuum oven.

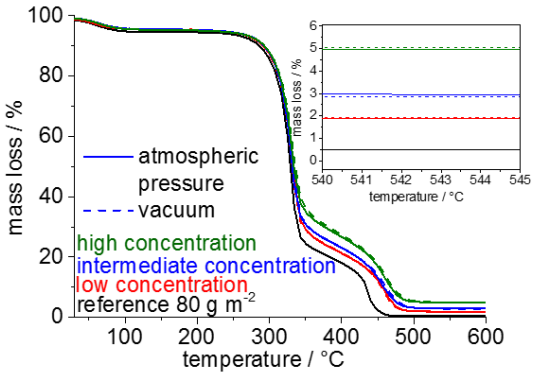


**Figure 3.** Thermogravimetric analysis of silica-coated eucalyptus sulfate paper (80 g $m^{-2}$) sheets. The amount of coating is determined by the TEOS concentration in the initial coating (red, blue and green) and, to a much smaller degree, by the curing process (atmospheric pressure = line and vacuum = dotted line).

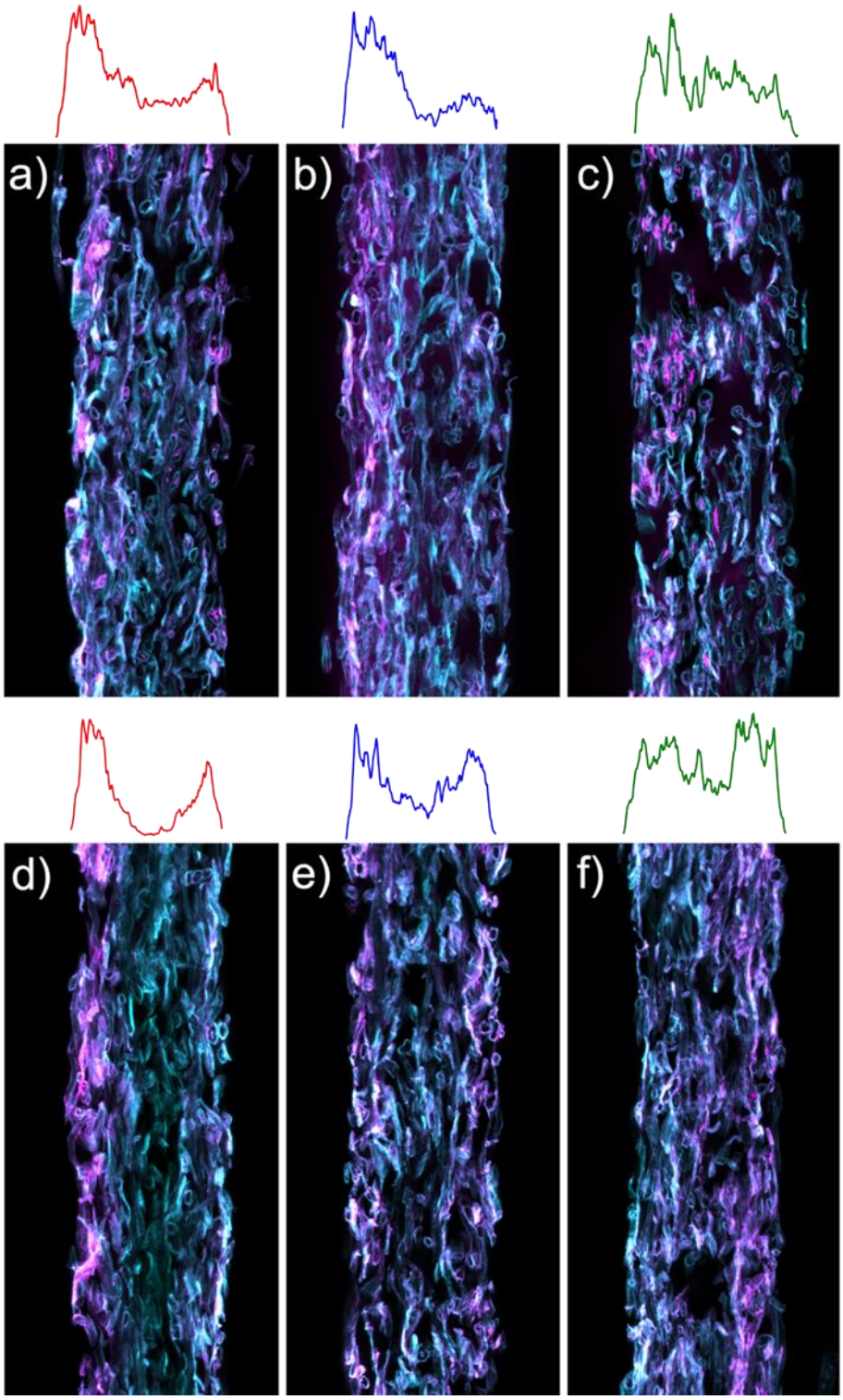


**Figure 4.** CLSM images of cross-sections of prepared hybrid papers and the corresponding relative silica distribution of a) samples prepared with a low TEOS concentration and cured under ambient pressure, b) samples prepared with an intermediate TEOS concentration and cured under ambient pressure, c) samples prepared with a high TEOS concentration and cured under ambient pressure, d) samples prepared with a low TEOS concentration and cured under vacuum, e) samples prepared with an intermediate TEOS concentration and cured under vacuum, and f) samples prepared with a high TEOS concentration and cured under vacuum. All images are z-projections of stacks with 20 to 25 individual images.

The table of contents entry should be 50–60 words long and should be written in the present tense and impersonal style (i.e., avoid we). The text should be different from the abstract text.

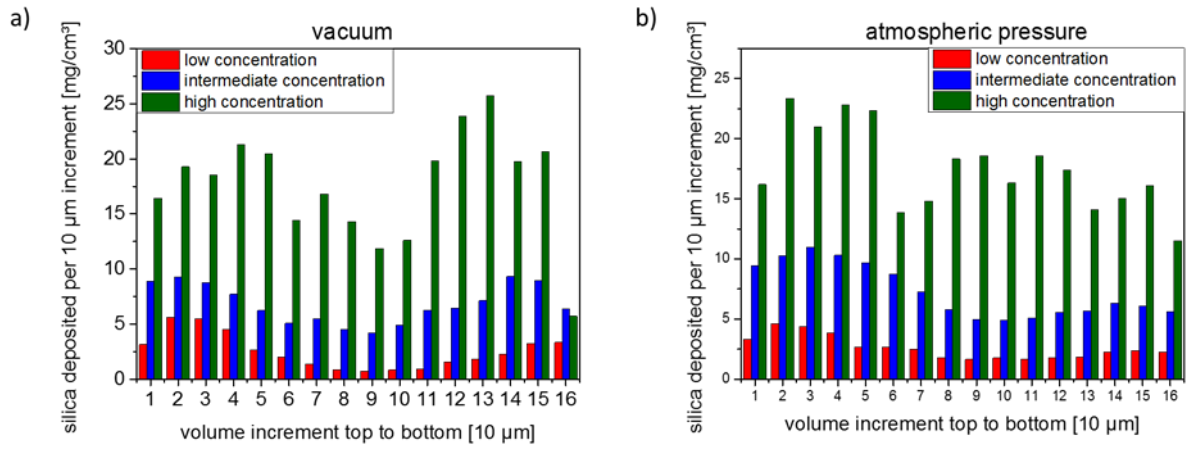


**Figure 5.** Absolute amount of silica per volume increment calculated through correlation of CLSM and TGA data for a) samples cured under vacuum and b) samples cured under ambient pressure.

| a) | **water permeation** | **no water permeation** |
|---|---|---|
| **oil permeation** | intermediate silica concentration (hydrophobic surface on water fraction) -> c) | high silica concentration -> d) |
| **no oil permeation** | low silica concentration -> e) | intermediate silica concentration (hydrophobic surface to oil fractions) -> f) |

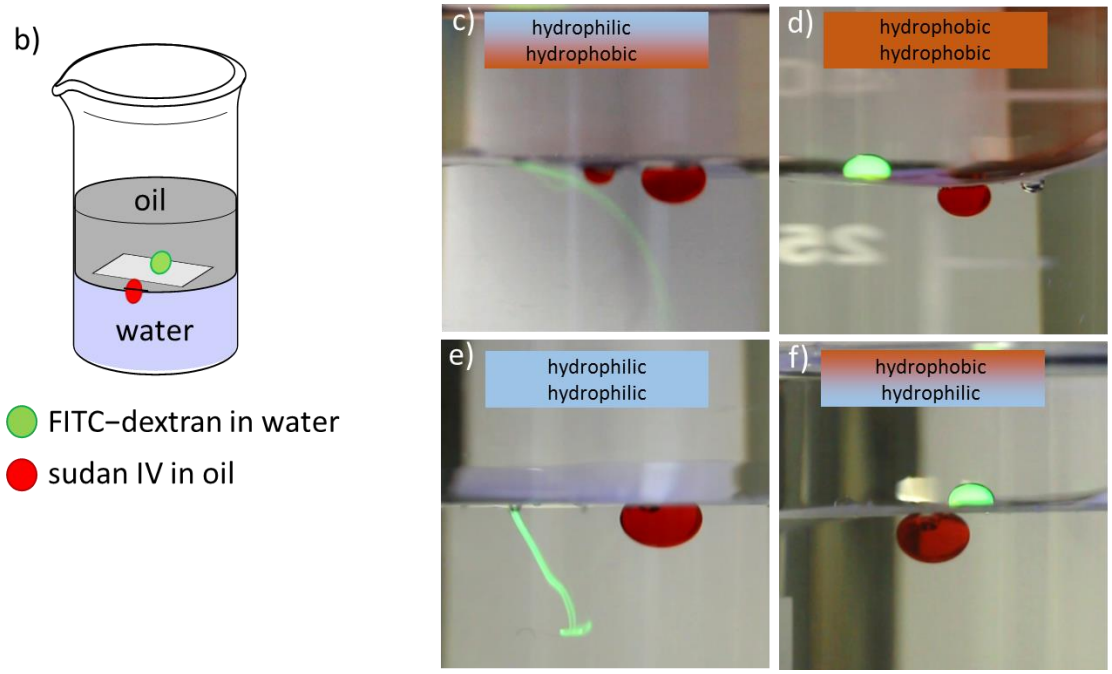


**Figure 6.** a) Table showing the oil/water infiltration or exclusion through different eucalyptus paper sheets prepared with different amounts of silica coating cured under atmospheric pressure. b) Experimental setup with a membrane between the water phase on the bottom and oil phase on the top. An oil droplet colored with Sudan IV or a water droplet colored with

FITC-dextran was positioned on the opposite side to look at droplet permeation. Images of the four combinations of permeation/exclusion are shown in c) through f): c) Janus membrane, where the hydrophobic interface lays on the water phase. d) Hydrophobic silica-coated paper membrane e) hydrophilic silica-coated paper and f) Janus membrane, where the hydrophilic interface lays on the water phase. Time dependent images of the systems are provided in **Figure S3**.

The table of contents entry:

Paper-based hybrid membranes with tailored chemical and wetting gradients along the paper sheet cross section are obtained from a simple and scalable one-step fabrication process using industry-compatible components. Gradient and Janus-type wettability result from a new mechanism based on cellulose fiber nanoporosity reduction. The novel process and resulting materials are of huge technological potential, as demonstrated for simple oil-water separation.

**Keyword** hybrid paper membrane

*Maximilian Nau, Nicole Herzog, Johannes Schmidt, Tobias Meckel, Annette Andrieu-Brunsen*, Markus Biesalski**

**Janus-Type Hybrid Paper Membranes**